

**Advanced deep learning methodology for accurate, real-time segmentation of high-resolution intravascular ultrasound images**

Retesh Bajaj, MBBS, BSc;<sup>1,2,#</sup> Xingru Huang, BEng;<sup>3,#</sup> Yakup Kilic, MD;<sup>1</sup> Anantharaman Ramasamy, MBChB;<sup>1,2</sup> Ajay Jain, MD;<sup>1</sup> Mick Ozkor, MD;<sup>1</sup> Vincenzo Tufaro, MD;<sup>1</sup> Hannah Safi, PhD;<sup>4</sup> Emrah Erdogan, MD;<sup>1</sup> Patrick W. Serruys, MD, PhD;<sup>5</sup> James Moon, MD;<sup>1,6</sup> Francesca Pugliese, MD, PhD;<sup>1,2</sup> Anthony Mathur, MD, PhD;<sup>1,2</sup> Ryo Torii, MSc, PhD;<sup>4</sup> Andreas Baumbach, MD, PhD;<sup>1,2</sup> Jouke Dijkstra, PhD;<sup>7</sup> Qianni Zhang, PhD;<sup>3</sup> Christos V. Bourantas, MD, PhD<sup>1,2,6,\*</sup>

<sup>1</sup> Department of Cardiology, Barts Heart Centre, Barts Health NHS Trust, London, UK

<sup>2</sup> Cardiovascular Devices Hub, Centre for Cardiovascular Medicine and Devices, William Harvey Research Institute, Queen Mary University of London, UK

<sup>3</sup> School of Electronic Engineering and Computer Science, Queen Mary University of London, UK

<sup>4</sup> Department of Mechanical Engineering, University College London, London, UK

<sup>5</sup> Faculty of Medicine, National Heart & Lung Institute, Imperial College London, UK

<sup>6</sup> Institute of Cardiovascular Sciences, University College London, London, UK

<sup>7</sup> Department of Radiology, Division of Image Processing, Leiden University Medical Center, Leiden, The Netherlands

# The 1<sup>st</sup> and 2<sup>nd</sup> author contributed equally to this work.

**Short title:** Advanced deep learning for accurate IVUS segmentation

**Conflicts of interests:** All authors have no conflicts of interests to declare.

**\*Address for correspondence**

Dr Christos V. Bourantas MD PhD

Consultant Cardiologist, Barts Heart Centre, West Smithfield, London EC1A 7BE

E-mail: [cbourantas@gmail.com](mailto:cbourantas@gmail.com), Phone: +44 203 765 8740

**Word Count:** 3, 349

## **Abstract**

**Aims:** The aim of this study is to develop and validate a deep learning (DL) methodology capable of automated and accurate segmentation of intravascular ultrasound (IVUS) image sequences in real-time.

**Methods and results:** IVUS segmentation was performed by two experts who manually annotated the external elastic membrane (EEM) and lumen borders in the end-diastolic frames of 197 IVUS sequences portraying the native coronary arteries of 65 patients. The IVUS sequences of 177 randomly-selected vessels were used to train and optimise a novel DL model for the segmentation of IVUS images. Validation of the developed methodology was performed in 20 vessels using the estimations of two expert analysts as the reference standard.

The mean difference for the EEM, lumen and plaque area between the DL-methodology and the analysts was  $\leq 0.23\text{mm}^2$  (standard deviation  $\leq 0.85\text{mm}^2$ ), while the Hausdorff and mean distance differences for the EEM and lumen borders was  $\leq 0.19\text{mm}$  (standard deviation  $\leq 0.17\text{mm}$ ). The agreement between DL and experts was similar to experts' agreement (Williams Index ranges: 0.754-1.061) with similar results in frames portraying calcific plaques or side branches.

**Conclusions:** The developed DL-methodology appears accurate and capable of segmenting high-resolution real-world IVUS datasets. These features are expected to facilitate its broad adoption and enhance the applications of IVUS in clinical practice and research.

**Keywords:** Intravascular ultrasound; image segmentation; machine learning.

## **Introduction**

Intravascular ultrasound (IVUS) is the preferred modality for assessing lumen and vessel wall dimensions, quantifying plaque burden and guiding revascularisation in complex lesions and high-risk patients.[1] Cumulative data have underscored its value in optimising procedural results and improving outcomes in patients undergoing percutaneous coronary intervention (PCI).[2–4] Its broader use, however, has been limited by the time and cost needed for acquiring and analysing IVUS imaging. Whilst several automated solutions have been proposed to aid IVUS segmentation, none has proven capable of processing IVUS images and accurately identifying the external elastic membrane (EEM) and lumen borders in real-time while the patient is in the cardiac catheterisation laboratory.[5]

Deep learning (DL) methodologies have begun to find medical application in facilitating the rapid and accurate processing of large imaging datasets. They rely on learning from large datasets of human annotations and use this information to train algorithmic models capable of processing images and replicating human performance within a few seconds.[6,7] These features render DL as the ideal approach for the analysis of IVUS images that have increased noise and artefacts which can confound conventional image-based segmentation approaches. Despite the undoubted theoretical advantages of DL methodologies in this setting, few studies have tested their potential value in IVUS analysis, mainly in small datasets providing promising results (Supplementary Table 1).[8–17] The aim of this study is to develop and validate a DL-methodology capable of automatically and accurately segmenting IVUS data in real-time.

## **Methods**

### *Study Population*

Seventy patients who provided written, informed consent were recruited to the “Evaluation of the efficacy of computed tomographic coronary angiography in assessing coronary artery morphology and physiology” study (NCT03556644) and included in this analysis. The rationale and the study design have been presented in detail previously.[18] All patients had stable angina due to atherosclerosis detected on cardiac catheterisation and were referred to Barts Heart Centre for further invasive assessment and therapy. Before repeat catheterisation, all patients underwent computed tomography

coronary angiography (CTCA). During coronary catheterisation near-infrared spectroscopy (NIRS)-IVUS imaging of the major epicardial vessels was performed. The study protocol complied with the Declaration of Helsinki and received approval from the local research ethics committee.

#### *Intravascular ultrasound data acquisition and analysis*

NIRS-IVUS imaging was performed in all three epicardial coronary arteries using the 2.4F 50MHz Dualpro system (Infraredx, Burlington, MA); in case of anatomical variation, the major epicardial vessels were selected for study. Intra-coronary isosorbide dinitrate (400mcg) was administered and the NIRS-IVUS probe was advanced to the distal vessel under angiographic guidance; images were acquired at 30fps as the probe was withdrawn at a fixed speed of 0.5mm/s using an automated pullback device.

Intravascular image analysis was performed by two well-trained analysts (RB and YK); all analyses were reviewed by an expert analyst (CVB) and corrections were made by consensus. First the end-diastolic frames were retrospectively-identified using an automated methodology that takes into account the relative movement of the NIRS-IVUS probe within the lumen to find the frame that corresponds to the peak of R-wave.[19] These frames were then segmented in accordance with previously published guidelines;[20] in each frame the EEM and lumen borders were detected using the QCU-CMS software (Version 4.69, Leiden, University Medical Center, Leiden, The Netherlands). Frames portraying stented segments were excluded from the analysis while in frames portraying calcific plaques obscuring  $\geq 90^\circ$  of the EEM border, only the lumen border was detected.

Ninety percent of the annotated IVUS pullbacks were randomly selected and used to train the DL-methodology (training set), while the remaining 10% were used for validation purposes (test set). In the test set, IVUS segmentation was performed twice by the first analyst (RB) within a 4-month interval for assessment of intra-observer variability, and once by the second analyst (YK) for assessment of inter-observer variability. The annotated images were extracted in the DICOM format at 480x480 pixels and converted to 256x256 pixels before being passed into the DL model.

#### *Training of the deep learning methodology*

The proposed segmentation methodology relies on a DL model built on the ResNet architecture (a convolutional neural network) that utilises the Pix2pix conditional generative adversarial network

(GAN).[21,22] Hyperparameter values were set empirically: L1 loss was used for the generator, while the loss generated by the generator and discriminator were added together as the final loss. The ratio between generative network and discriminative network was 100:1. Based on the GAN structure, a fixed learning rate of  $1e^{-4}$  was applied. The batch size was set to 16 with maximum training epochs of 200. Model parameter values were directly learned from the data. As the process does not involve any parameter fine-tuning, a discrete validation set was not used. The configuration of the PC used in this study was: Xeon 1660 v3 CPU with 2 x 2080Ti graphics cards.

A schematic representation of the process is shown in Figure 1. The model is designed to estimate EEM and lumen borders obscured by calcific shadowing or ambiguity due to side-branches by taking into account expert analysts' annotations. Given the morphological differences of the EEM and lumen borders, a separate model was trained for each.

The annotated dataset initially undergoes augmentation with random rotations, cropping, re-scaling and brightness adjustment. This process increases the number of annotated frames used for training purposes. The training of the model for the EEM border detection involves the analysis of every annotated end-diastolic frame sequentially and the extraction of deep features that generate a mask of the annotation which is compared to the original annotation. This process is iteratively repeated, changing and improving the model, until the mask generated is highly accurate compared to the original annotation. The updated model then moves on to the next annotated frame and the process repeats in sequence until all end-diastolic frames have been used for training.

The identification of the lumen border is more challenging in IVUS images than the EEM border.[23] The border is searched for in the area defined by the EEM and its detection involves generation of three fused images for each end-diastolic frame to train the model. These are the annotated mask of the lumen, a composite of 2 frames before and after this frame, and finally a composite of 1 frame before and after with digital subtraction; the latter images enable identification of the moving red blood cell speckles and thus differentiation of the lumen from the intima. The lumen model is sequentially trained in the generated fused images using the estimations of the analysts as reference standard.

The trained model was then tested in the test set. In this set, the estimations of the model were compared with the annotations of the analysts. To generate more stable and accurate borders each end-diastolic

frame was transformed to generate a set of 9 additional images: 3 with a similar size that were produced after random rotation of the original frame, 3 with 20% smaller size and 3 with 20% larger size. The model processed the original and the 9 additional frames, identified the EEM and lumen borders and these were reversed to the original dimensions when needed. The 10 borders were then averaged to generate the final contour for each input image which included the pixels enclosed by the EEM or the lumen contours in at least 3 out of the 10 annotations. This fusion step was performed to overcome potential errors that may have occurred in each of the 10 annotations and thus produce a more accurate final estimation.

### *Statistical Methods*

Numerical values are presented as mean $\pm$ standard deviation (SD) while categorical values as absolute values and percentages. To compare the performance of the DL-methodology and the analysts several metrics were used. The EEM, lumen and plaque areas (defined as: EEM – lumen area) were measured in every annotated frame and compared using Spearman's rank correlation coefficient, linear regression and Bland-Altman analysis. Morphological comparative metrics comprising the Dice similarity coefficient (DSC), the intersection over union ratio (IOU/Jaccard Index), the Hausdorff distance and mean distance were estimated after superimposing the DL-methodology's and the analysts' estimations for the EEM and lumen borders (Supplementary Figure 1).[24,25] The DSC and the IUO analyses represent the pixel-level degree of similarity between two annotations and range from 0 (no similarity) to 1 (identical). The Hausdorff distance was calculated as the maximal distance and the mean distance as the average distance between two superimposed annotations. To assess the performance of the DL-method in challenging frames, analysis was separately performed for those portraying the origin of a side-branch of at least 1.5mm and for those with calcific plaques obscuring  $\geq 30^\circ$  of the EEM (Supplementary Figure 2). The same metrics were used to assess the intra- and inter-observer variability of the expert analysts.

To examine whether the DL-methodology is as accurate as the two expert analysts in segmenting IVUS frames the Williams Index (WI) and its 95% confidence interval were assessed and reported for all the measured metrics.[24] The WI was introduced to compare the variation between a method of unknown accuracy (i.e., the DL-methodology) and the established expert analysts with the variation between the

two analysts. A WI close to unity suggests that the differences between the estimations of the DL-method and the ones obtained by the analysts are not larger than their inter-observer variability indicating that the tested method is as accurate as the analysts. Statistical analyses were performed using SPSS 26 (IBM, Armonk, New York).

## **Results**

NIRS-IVUS was performed in 65 (197 vessels; 3.03 vessels/patient) out of 70 recruited patients; one patient was excluded due to acute kidney injury post CTCA, one patient was excluded due to findings of a thymoma on CTCA and three cases due to NIRS-IVUS catheter dysfunction. The baseline demographics of the studied patients and the output of the IVUS analysis are shown in Supplementary Table 2 and 3 respectively.

The training set consisted of 824,750 frames (177 vessels), of which 23,774 end-diastolic frames were analysed. The test set consisted of 84,737 frames (20 vessels), including 2,437 end-diastolic frames (241 frames portraying the origin of a side-branch  $\geq 1.5\text{mm}$  and 229 portraying a calcific plaque with  $\geq 30^\circ$  calcific arc shadow obscuring the EEM border) which were selected for segmentation.

Manual segmentation of the end-diastolic frames in a representative 5000-frame pullback took approximately 9 hours; conversely, the DL-methodology was able to segment this vessel in 2 minutes using a desktop PC with an Intel Core i5 processor and 8 GB of RAM.

### *Intra- and inter-observer variability*

The inter and intra-observer variability of the expert analysts is shown in Table 1 and Supplementary Tables 4-6. A high correlation was noted between the 1<sup>st</sup> analyst's annotations and between the 1<sup>st</sup> and 2<sup>nd</sup> analysts' estimations for the EEM, lumen and plaque areas while linear regression analyses yielded slopes close to 1 and y-intercepts close to 0 (Figure 2). The mean differences between 1<sup>st</sup> analyst's estimations and between the estimations of the two analysts were  $\leq 0.17\text{mm}^2$  (SD  $\leq 0.74\text{mm}^2$ ) for the EEM, lumen and plaque areas.

A morphological evaluation of analysts' agreement also showed low intra- and inter-observer variability. For the EEM borders, the DSC and IOU indices were close to 1, while the average HD and mean distance values was  $\leq 0.13\text{mm}$  and  $\leq 0.03\text{mm}$ , respectively. For the lumen borders, there were

marginally greater morphological differences but strong agreement again, with DSC and IOU  $\geq 0.93$  while the HD and the mean distance values were  $\leq 0.18\text{mm}$  (SD  $\leq 0.13\text{mm}$ ) and  $\leq 0.05\text{mm}$  (SD  $\leq 0.04\text{mm}$ ), respectively (Table 1).

#### *Quantitative evaluation of EEM and lumen segmentation by the DL-methodology*

A high correlation was found between the estimations of the DL-method and the analysts for the EEM, lumen and plaque areas ( $r \geq 0.975$  for all the studied variables). Linear regression analyses also showed a high agreement between DL-method and the analysts while Bland-Altman analysis demonstrated a minimal bias with mean differences  $\leq 0.08\text{mm}^2$  (SD  $\leq 0.80\text{mm}$ ) for the EEM,  $\leq 0.21\text{mm}^2$  (SD  $\leq 0.63\text{mm}$ ) for the lumen and  $\leq 0.23\text{mm}^2$  (SD  $\leq 0.85\text{mm}$ ) for the plaque area estimations (Figure 3). The WI was 0.754 for the EEM area while for the lumen and plaque areas it was 0.950 and 0.951, respectively (Table 1).

#### *Morphological evaluation of external elastic membrane and lumen segmentation by the deep learning methodology*

A morphological evaluation of the DL-methodology demonstrated a high agreement with the analysts' annotations that were treated as the reference standard. The DSC and IOU ranged from 0.96-0.98 and 0.92-0.96, respectively while the range for the HD and mean distance was 0.15-0.19mm and 0.04-0.06mm, respectively. WI analyses confirmed that the annotations of the DL-methodology were as reliable as the two analysts' estimations as the indices ranged from 0.86-1.06.

Results were not different when analysis focused in frames without calcified plaque or side branches (Supplementary table 4). Conversely, in frames portraying the origin of side branches there was a marginally higher difference between the estimations of the DL-methodology and the analysts for the EEM area, while for the lumen and plaque areas the WI was 1.020 and 0.925, respectively indicating that the proposed method is as accurate as the analysts for assessing lumen and plaque dimensions in these frames (Supplementary Table 5). Similarly, in frames portraying calcified plaque the WI was higher for the EEM area comparing to frames without calcific tissue but there were no differences for the WI estimations for the lumen and plaque area (Supplementary Table 6).

## Discussion

In the present study we developed a novel DL-methodology and examined its efficacy in detecting the EEM and lumen borders in high-resolution IVUS images. The methodology was trained in a large dataset of 177 vessels and tested in 20 vessels. Both sets included frames portraying common artifacts seen in IVUS (guide-wire artifacts, non-uniform rotational distortion, motion artifacts, reverberations, side lobe artifacts and blood speckle artifacts) as well as frames with calcific tissue and side branches. The reported results indicate that the proposed methodology is capable of accurately segmenting high-resolution IVUS sequences in a few minutes enabling its real-time application in the catheterisation laboratory. The automated analysis of IVUS images has been an unmet challenge in interventional research. Over the last 25 years several automated segmentation methodologies have been developed that incorporated edge-tracking and gradient based techniques,[26–29] snake models,[30–33] probabilistic-based approaches,[34] or multiscale expansion-based methodologies[35] for the detection of the EEM and lumen borders. Although validation of most of the proposed methodologies have shown promising results in small datasets[25] they have failed to dominate in clinical practice. This can be attributed to the increased time required for such analysis (as some of them require processing of the entire IVUS sequence), the inability to successfully segment images with artefacts that are often seen in IVUS and to detect the EEM in images with calcified plaques that generate acoustic shadowing obscuring the EEM border. Therefore, IVUS analysis is currently performed by expert analysts who manually annotate the EEM and lumen borders in the frames of interest. This process however is laborious, time-consuming and relies on analysts' expertise, all of which limit the application of IVUS in clinical practice. Moreover, the increased time required for the analysis of IVUS images has restricted the applications of this modality in research as IVUS clinical studies require manpower and funding support for the analysis of the obtained data.

Deep and machine-learning techniques have been recognised as useful approaches in medical image analysis and have been extensively used to automatically process large imaging data.[7] Nevertheless the applications of DL-methodologies for the processing of IVUS imaging data are limited.[8–17] This is due to the small number of IVUS annotations used for training that did not allow full development of the model,[8–13] methodologies not being designed to segment both EEM and lumen borders thus

not being able to analyse the plaque burden and volume,[17] the limited efficacy of the proposed methods in accurately detecting the lumen border,[14,16] the inability of the existing methods to process challenging IVUS frames with side branches and increased calcific burden and to the fact that the developed algorithms have not been tested in large datasets so as to have objective evidence about their efficacy and potential value in clinical practice.[8–13]

In the present study we introduce an advanced DL-based segmentation method which appears able to overcome the above limitations. For the first time, we used a large number of high-resolution IVUS images to train a DL-methodology that is based on the ResNet neural network and takes advantage of the adjacent IVUS frames to accurately detect the EEM and lumen borders in IVUS frames. Validation in 20 vessels showed that the proposed method is capable of accurately segmenting IVUS images and estimate lumen and plaque area with a high accuracy that is similar – as shown by the WI values – to the efficacy of expert analysts. When analysis focused in challenging cases, such as frames portraying the origin of side branches or calcific plaques, we found that the DL-methodology performed well and that was as accurate as the analysts in assessing plaque area.

Conversely, we found relatively lower WI values in EEM area estimations due to the high agreement between analysts, rather than a large difference between manual annotations and the estimations of the DL-methodology. A morphological analysis of DL-estimations confirmed the geometrical similarity of the EEM and lumen estimations with the borders delineated by the two analysts. The proposed methodology also appears capable of processing IVUS sequences acquired by other systems; the results from its application in a phased array 20MHz IVUS dataset in public domain compares favourably with those reported in the literature (Supplementary Table 1).[25]

Another advantage of the developed method is the fact that it is expeditious: enabling analysis of a 30mm coronary segment in approximately 60s, allowing its use in clinical practice. Incorporation of the proposed method in IVUS systems is expected to allow real-time segmentation of an IVUS sequence and quantification of the lumen and vessel wall dimensions allowing optimal PCI planning. Further processing of the annotated borders with computational fluid dynamic techniques are anticipated to allow accurate estimation of the pressure gradient across a lesion and thus, similar to optical coherence tomography-based software,[36] detection of flow-limiting stenoses. Currently, the proposed

methodology has been incorporated in the QCU-CMS software, widely used for IVUS research analysis and is expected to facilitate and expedite rapid analysis of large IVUS datasets. In the future we aim to train and test its performance in lower-resolution IVUS images (i.e., 40MHz IVUS) expand its application in the analysis of stented coronary segments as well as incorporate automated detection and measurement of the arc of calcification.

### *Limitations*

The proposed methodology has been trained and validated only in 50MHz IVUS sequences, therefore the reported results cannot be extrapolated to other IVUS data. However, the findings from the analysis of the public domain 20MHz IVUS dataset indicate that it can have application for the analysis of IVUS images acquired by different IVUS systems. Another significant limitation is the fact that the data that used for the training and validation of the DL-methodology did not include stented segments and thus we did not develop algorithms for the detection of the stent border. Therefore, further analysis and developments are needed before this methodology has application in stented segments including automatic detection of stent borders, quantification of neointima burden and identification of malapposition.

### **Conclusions**

In the present study we present for the first time a novel DL-methodology that is capable of accurate, automated segmentation of high-resolution IVUS images in real-time. An extensive morphological and quantitative validation in a large dataset has demonstrated that the proposed method is able to overcome common artefacts seen in IVUS and segment challenging frames portraying the origin of side branches and calcific plaques. These features are expected to facilitate its broad adoption and enhance the applications of IVUS in clinical practice and research.

### **Acknowledgements**

The authors wish to acknowledge the Cardiovascular Devices Hub at the Centre for Cardiovascular Medicine and Devices, Queen Mary University of London for supporting the present study.

**Sources of funding**

This study is jointly funded by British Heart Foundation (PG/17/18/32883), University College London Biomedical Resource Centre (BRC492B) and Rosetrees Trust (A1773). RB, AR, VT, AM, AB and CVB are funded by Barts NIHR Biomedical Research Centre, London, UK.

**Conflicts of interests**

All authors have no conflicts of interests to declare.

## References

- [1] G.S. Mintz, G. Guagliumi, Intravascular imaging in coronary artery disease, *The Lancet*. 390 (2017) 793–809. [https://doi.org/10.1016/S0140-6736\(17\)31957-8](https://doi.org/10.1016/S0140-6736(17)31957-8).
- [2] D.-H. Shin, S.-J. Hong, G.S. Mintz, J.-S. Kim, B.-K. Kim, Y.-G. Ko, D. Choi, Y. Jang, M.-K. Hong, Effects of Intravascular Ultrasound-Guided Versus Angiography-Guided New-Generation Drug-Eluting Stent Implantation: Meta-Analysis With Individual Patient-Level Data From 2,345 Randomized Patients, *JACC Cardiovasc Interv.* 9 (2016) 2232–2239. <https://doi.org/10.1016/j.jcin.2016.07.021>.
- [3] S.-J. Hong, G.S. Mintz, C.-M. Ahn, J.-S. Kim, B.-K. Kim, Y.-G. Ko, T.-S. Kang, W.-C. Kang, Y.H. Kim, S.-H. Hur, B.-K. Hong, D. Choi, H. Kwon, Y. Jang, M.-K. Hong, IVUS-XPL Investigators, Effect of Intravascular Ultrasound-Guided Drug-Eluting Stent Implantation: 5-Year Follow-Up of the IVUS-XPL Randomized Trial, *JACC Cardiovasc Interv.* 13 (2020) 62–71. <https://doi.org/10.1016/j.jcin.2019.09.033>.
- [4] Y. Zhang, V. Farooq, H.M. Garcia-Garcia, C.V. Bourantas, N. Tian, S. Dong, M. Li, S. Yang, P.W. Serruys, S.-L. Chen, Comparison of intravascular ultrasound versus angiography-guided drug-eluting stent implantation: a meta-analysis of one randomised trial and ten observational studies involving 19,619 patients, *EuroIntervention.* 8 (2012) 855–865. <https://doi.org/10.4244/EIJV8I7A129>.
- [5] A. Katouzian, E.D. Angelini, S.G. Carlier, J.S. Suri, N. Navab, A.F. Laine, A State-of-the-Art Review on Segmentation Algorithms in Intravascular Ultrasound (IVUS) Images, *IEEE Transactions on Information Technology in Biomedicine.* 16 (2012) 823–834. <https://doi.org/10.1109/TITB.2012.2189408>.
- [6] Henglin Mir, Stein Gillian, Hushcha Pavel V., Snoek Jasper, Wiltschko Alexander B., Cheng Susan, Machine Learning Approaches in Cardiovascular Imaging, *Circulation: Cardiovascular Imaging.* 10 (2017) e005614. <https://doi.org/10.1161/CIRCIMAGING.117.005614>.
- [7] S.J. Al’Aref, K. Anchouche, G. Singh, P.J. Slomka, K.K. Kolli, A. Kumar, M. Pandey, G. Maliakal, A.R. van Rosendaal, A.N. Beecy, D.S. Berman, J. Leipsic, K. Nieman, D. Andreini, G. Pontone, U.J. Schoepf, L.J. Shaw, H.-J. Chang, J. Narula, J.J. Bax, Y. Guan, J.K. Min, Clinical applications

- of machine learning in cardiovascular disease and its relevance to cardiac imaging, *European Heart Journal*. 40 (2019) 1975–1986. <https://doi.org/10.1093/eurheartj/ehy404>.
- [8] J. Yang, M. Faraji, A. Basu, Robust segmentation of arterial walls in intravascular ultrasound images using Dual Path U-Net, *Ultrasonics*. 96 (2019) 24–33. <https://doi.org/10.1016/j.ultras.2019.03.014>.
- [9] S. Su, Z. Hu, Q. Lin, W.K. Hau, Z. Gao, H. Zhang, An artificial neural network method for lumen and media-adventitia border detection in IVUS, *Computerized Medical Imaging and Graphics*. 57 (2017) 29–39. <https://doi.org/10.1016/j.compmedimag.2016.11.003>.
- [10] J. Yang, L. Tong, M. Faraji, A. Basu, IVUS-Net: An Intravascular Ultrasound Segmentation Network, in: A. Basu, S. Berretti (Eds.), *Smart Multimedia*, Springer International Publishing, Cham, 2018: pp. 367–377. [https://doi.org/10.1007/978-3-030-04375-9\\_31](https://doi.org/10.1007/978-3-030-04375-9_31).
- [11] L. Lo Vercio, M. Del Fresno, I. Larrabide, Lumen-intima and media-adventitia segmentation in IVUS images using supervised classifications of arterial layers and morphological structures, *Comput Methods Programs Biomed*. 177 (2019) 113–121. <https://doi.org/10.1016/j.cmpb.2019.05.021>.
- [12] M. Xia, W. Yan, Y. Huang, Y. Guo, G. Zhou, Y. Wang, IVUS images segmentation using spatial fuzzy clustering and hierarchical level set evolution, *Computers in Biology and Medicine*. 109 (2019) 207–217. <https://doi.org/10.1016/j.combiomed.2019.04.029>.
- [13] J. Yang, J. Li, N. Dai, J. Ma, H. Lan, L. Zheng, J. Ge, TCT-352 Deep Learning–Based Fully Automated Segmentation of IVUS for Quantitative Measurement, *Journal of the American College of Cardiology*. 74 (2019) B349. <https://doi.org/10.1016/j.jacc.2019.08.436>.
- [14] D. Molony, H. Hosseini, H. Samady, TCT-2 Deep IVUS: A machine learning framework for fully automatic IVUS segmentation, *J Am Coll Cardiol*. 72 (2018) B1. <https://doi.org/10.1016/j.jacc.2018.08.1077>.
- [15] D. Mishra, S. Chaudhury, M. Sarkar, A.S. Soin, Ultrasound Image Segmentation: A Deeply Supervised Network With Attention to Boundaries, *IEEE Transactions on Biomedical Engineering*. 66 (2019) 1637–1648. <https://doi.org/10.1109/TBME.2018.2877577>.

- [16] S. Kim, Y. Jang, B. Jeon, Y. Hong, H. Shim, H. Chang, Fully Automatic Segmentation of Coronary Arteries Based on Deep Neural Network in Intravascular Ultrasound Images, in: D. Stoyanov, Z. Taylor, S. Balocco, R. Sznitman, A. Martel, L. Maier-Hein, L. Duong, G. Zahnd, S. Demirci, S. Albarqouni, S.-L. Lee, S. Moriconi, V. Cheplygina, D. Mateus, E. Trucco, E. Granger, P. Jannin (Eds.), *Intravascular Imaging and Computer Assisted Stenting and Large-Scale Annotation of Biomedical Data and Expert Label Synthesis*, Springer International Publishing, Cham, 2018: pp. 161–168. [https://doi.org/10.1007/978-3-030-01364-6\\_18](https://doi.org/10.1007/978-3-030-01364-6_18).
- [17] P.G.P. Ziemer, C.A. Bulant, J.I. Orlando, G.D. Maso Talou, L.A.M. Álvarez, C. Guedes Bezerra, P.A. Lemos, H.M. García-García, P.J. Blanco, Automated lumen segmentation using multi-frame convolutional neural networks in intravascular ultrasound datasets, *Eur Heart J Digit Health*. 1 (2020) 75–82. <https://doi.org/10.1093/ehjdh/ztaa014>.
- [18] A. Ramasamy, H. Safi, J.C. Moon, M. Andiapen, K.S. Rathod, P. Maurovich-Horvat, R. Bajaj, P.W. Serruys, A. Mathur, A. Baumbach, F. Pugliese, R. Torii, C.V. Bourantas, Evaluation of the Efficacy of Computed Tomographic Coronary Angiography in Assessing Coronary Artery Morphology and Physiology: Rationale and Study Design, *Cardiology*. 145 (2020) 285–293. <https://doi.org/10.1159/000506537>.
- [19] S.A. de Winter, R. Hamers, M. Degertekin, K. Tanabe, P.A. Lemos, P.W. Serruys, J.R.T.C. Roelandt, N. Bruining, A novel retrospective gating method for intracoronary ultrasound images based on image properties, in: *Computers in Cardiology, 2003*, IEEE, Thessaloniki Chalkidiki, Greece, 2003: pp. 13–16. <https://doi.org/10.1109/CIC.2003.1291078>.
- [20] G.S. Mintz, S.E. Nissen, R.A. O'Rourke, American College of Cardiology Clinical Expert Consensus Document on Standards for Acquisition, Measurement and Reporting of Intravascular Ultrasound Studies (IVUS). A report of the American College of Cardiology Task Force on Clinical Expert Consensus Documents., *Journal of the American College of Cardiology*. 37 (2001) 15.
- [21] P. Isola, J.-Y. Zhu, T. Zhou, A.A. Efros, Image-to-Image Translation with Conditional Adversarial Networks, *ArXiv:1611.07004 [Cs]*. (2018). <http://arxiv.org/abs/1611.07004> (accessed July 15, 2020).

- [22] Q. Zhang, Z. Cui, X. Niu, S. Geng, Y. Qiao, Image Segmentation with Pyramid Dilated Convolution Based on ResNet and U-Net, in: D. Liu, S. Xie, Y. Li, D. Zhao, E.-S.M. El-Alfy (Eds.), *Neural Information Processing*, Springer International Publishing, Cham, 2017: pp. 364–372. [https://doi.org/10.1007/978-3-319-70096-0\\_38](https://doi.org/10.1007/978-3-319-70096-0_38).
- [23] G.A. Rodriguez-Granillo, H.M. García-García, E.P. Mc Fadden, M. Valgimigli, J. Aoki, P. de Feyter, P.W. Serruys, In Vivo Intravascular Ultrasound-Derived Thin-Cap Fibroatheroma Detection Using Ultrasound Radiofrequency Data Analysis, *Journal of the American College of Cardiology*. 46 (2005) 2038–2042. <https://doi.org/10.1016/j.jacc.2005.07.064>.
- [24] V. Chalana, Y. Kim, A Methodology For Evaluation of Boundary Detection Algorithms on Medical Images, *IEEE Transactions on Medical Imaging*. (1997) 642–652.
- [25] S. Balocco, C. Gatta, F. Ciompi, A. Wahle, P. Radeva, S. Carlier, G. Unal, E. Sanidas, J. Mauri, X. Carillo, T. Kovarnik, C.-W. Wang, H.-C. Chen, T.P. Exarchos, D.I. Fotiadis, F. Destrempes, G. Cloutier, O. Pujol, M. Alberti, E.G. Mendizabal-Ruiz, M. Rivera, T. Aksoy, R.W. Downe, I.A. Kakadiaris, Standardized evaluation methodology and reference database for evaluating IVUS image segmentation, *Comput Med Imaging Graph*. 38 (2014) 70–90. <https://doi.org/10.1016/j.compmedimag.2013.07.001>.
- [26] C. von Birgelen, A. van der Lugt, A. Nicosia, G.S. Mintz, E.J. Gussenhoven, E. de Vrey, M.T. Mallus, J.R.T.C. Roelandt, P.W. Serruys, P.J. de Feyter, Computerized assessment of coronary lumen and atherosclerotic plaque dimensions in three-dimensional intravascular ultrasound correlated with histomorphometry, *The American Journal of Cardiology*. 78 (1996) 1202–1209. [https://doi.org/10.1016/S0002-9149\(96\)00596-6](https://doi.org/10.1016/S0002-9149(96)00596-6).
- [27] C. von Birgelen, C. Di Mario, W. Li, J.C.H. Schuurbiers, C.J. Slager, P.J. de Feyter, J.R.T.C. Roelandt, P.W. Serruys, Morphometric analysis in three-dimensional intracoronary ultrasound: An in vitro and in vivo study performed with a novel system for the contour detection of lumen and plaque, *American Heart Journal*. 132 (1996) 516–527. [https://doi.org/10.1016/S0002-8703\(96\)90233-1](https://doi.org/10.1016/S0002-8703(96)90233-1).
- [28] J. Dijkstra, G. Koning, J.C. Tuinenburg, P.V. Oemrawsingh, C. von Birgelen, J.H.C. Reiber, Automatic border detection in IntraVascular UltraSound images for quantitative measurements

- of the vessel, lumen and stent parameters, *International Congress Series*. 1230 (2001) 916–922.  
[https://doi.org/10.1016/S0531-5131\(01\)00155-8](https://doi.org/10.1016/S0531-5131(01)00155-8).
- [29] D.S. Meier, R.M. Cothren, D.G. Vince, J.F. Cornhill, Automated morphometry of coronary arteries with digital image analysis of intravascular ultrasound, *Am. Heart J.* 133 (1997) 681–690.  
[https://doi.org/10.1016/s0002-8703\(97\)70170-4](https://doi.org/10.1016/s0002-8703(97)70170-4).
- [30] M. Kass, A. Witkin, D. Terzopoulos, Snakes: Active contour models, *International Journal of Computer Vision*. 1 (1988) 321–331. <https://doi.org/10.1007/BF00133570>.
- [31] C.V. Bourantas, M.E. Plissiti, D.I. Fotiadis, V.C. Protopappas, G.V. Mpozios, C.S. Katsouras, I.C. Kourtis, M.R. Rees, L.K. Michalis, In vivo validation of a novel semi-automated method for border detection in intravascular ultrasound images, *Br J Radiol.* 78 (2005) 122–129.  
<https://doi.org/10.1259/bjr/30866348>.
- [32] G. Kovalski, R. Beyar, R. Shofti, H. Azhari, Three-dimensional automatic quantitative analysis of intravascular ultrasound images, *Ultrasound Med Biol.* 26 (2000) 527–537.  
[https://doi.org/10.1016/s0301-5629\(99\)00167-2](https://doi.org/10.1016/s0301-5629(99)00167-2).
- [33] Q. Zhang, Y. Wang, W. Wang, J. Ma, J. Qian, J. Ge, Automatic segmentation of calcifications in intravascular ultrasound images using snakes and the contourlet transform, *Ultrasound Med Biol.* 36 (2010) 111–129. <https://doi.org/10.1016/j.ultrasmedbio.2009.06.1097>.
- [34] E.G. Mendizabal-Ruiz, M. Rivera, I.A. Kakadiaris, Segmentation of the luminal border in intravascular ultrasound B-mode images using a probabilistic approach, *Med Image Anal.* 17 (2013) 649–670. <https://doi.org/10.1016/j.media.2013.02.003>.
- [35] A. Katouzian, B. Baseri, E.E. Konofagou, A.F. Laine, Automatic detection of blood versus non-blood regions on intravascular ultrasound (IVUS) images using wavelet packet signatures, in: *Medical Imaging 2008: Ultrasonic Imaging and Signal Processing*, International Society for Optics and Photonics, 2008: p. 69200H. <https://doi.org/10.1117/12.773600>.
- [36] J. Huang, H. Emori, D. Ding, T. Kubo, W. Yu, P. Huang, S. Zhang, J.L. Gutiérrez-Chico, T. Akasaka, W. Wijns, S. Tu, Comparison of Diagnostic Performance of Intracoronary Optical Coherence Tomography-based and Angiography-based Fractional Flow Reserve for Evaluation of Coronary Stenosis, *EuroIntervention*. (2020). <https://doi.org/10.4244/EIJ-D-19-01034>.

## Figure legends

**Figure 1.** Schematic representation of the developed DL-methodology. 1A: original IVUS sequence in training set (177 vessels) and annotated end-diastolic frames. 1B: definition of the EEM training set by selecting the annotated end-diastolic frames, augmentation of the dataset and training of the model. 1C: test set including end-diastolic frames in 20 vessels; these frames were then transformed to generate 10 images from each end-diastolic frame that are processed by the model which estimated the EEM border in each image. 1D: definition of the lumen training set by fusion of sequential frames before and after the annotated end-diastolic frame, augmentation of the dataset and training of the model. 1E: test set including end-diastolic frames in 20 vessels; these frames were then transformed to generate 10 images from each end-diastolic frame that are processed by the model which estimated the lumen border in each image. 1F: extraction of final EEM and lumen borders from the 10 estimations in each end-diastolic frame.

**Figure 2.** Intra- (2A-2C) and inter-observer (2D-2F) Bland-Altman, linear regression analysis and correlation coefficient ( $r$ ) comparing per-frame EEM, lumen and plaque cross-sectional areas in all annotated frames. The blue line represents the regression line and the limits of agreement ( $\pm 1.96SD$ ) are shown in red.

**Figure 3.** Bland-Altman, linear regression analysis and correlation coefficient ( $r$ ) comparing per-frame EEM, lumen and plaque cross-sectional area between the DL-methodology and expert analysts in all annotated frames. 3A-3C: comparing DL-methodology and the first analyst and 3D-3F: comparing DL-methodology and the second analyst. The blue line represents the regression line; the limits of agreement ( $\pm 1.96SD$ ) are shown in red.

**Table 1.** Quantitative and morphological comparison of the EEM and lumen annotations of the analysts and the DL-methodology in the test set.

		Analyst 1, 1 <sup>st</sup> estimation –	Analyst 1 –	DL-methodology –	DL-methodology –	Williams Index	
		analyst 1, 2 <sup>nd</sup> estimation	analyst 2	analyst 1	analyst 2	(95% CI)	
Quantitative	analysis	EEM area (mm <sup>2</sup> )	-0.09±0.46	0.10±0.53	-0.01±0.80	0.08±0.74	0.754 (0.752, 0.755)
		Lumen area (mm <sup>2</sup> )	0.07±0.47	-0.07±0.65	0.21±0.61	0.14±0.63	0.950 (0.949, 0.951)
		Plaque area (mm <sup>2</sup> )	-0.16±0.58	0.17±0.74	0.23±0.85	0.06±0.69	0.951 (0.950, 0.952)
Morphological analysis	EEM estimations	DSC	0.99±0.01	0.98±0.02	0.98±0.02	0.98±0.02	1.003 (1.003, 1.003)
		IOU	0.97±0.02	0.96±0.03	0.96±0.03	0.96±0.03	1.006 (1.006, 1.006)
		HD (mm)	0.11±0.11	0.13±0.13	0.15±0.17	0.15±0.17	0.884 (0.883, 0.884)
		Mean distance (mm)	0.03±0.03	0.03±0.04	0.04±0.04	0.04±0.04	0.857 (0.857, 0.858)
	Lumen estimations	DSC	0.97±0.02	0.96±0.02	0.96±0.03	0.96±0.03	1.003 (1.003, 1.003)
		IOU	0.94±0.04	0.93±0.04	0.92±0.05	0.92±0.05	1.006 (1.006, 1.006)
		HD (mm)	0.16±0.11	0.18±0.13	0.19±0.15	0.19±0.16	1.061 (1.060, 1.061)
		Mean distance (mm)	0.04±0.03	0.05±0.04	0.06±0.04	0.06±0.04	1.032 (1.031, 1.032)

**Table Footnote:** CI, confidence interval; DL, deep learning; DSC, Dice similarity coefficient; EEM, external elastic membrane; HD, Hausdorff distance;

IOU, intersection over union.

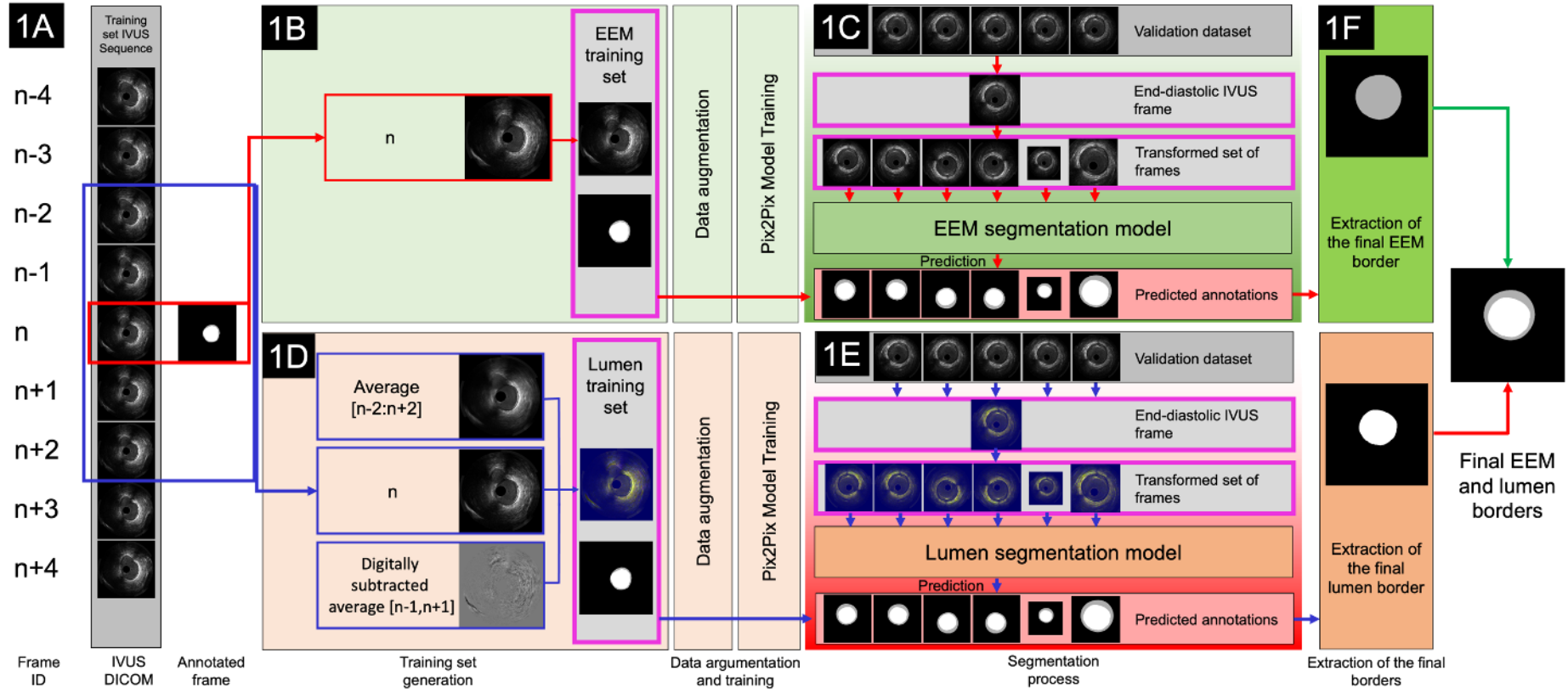
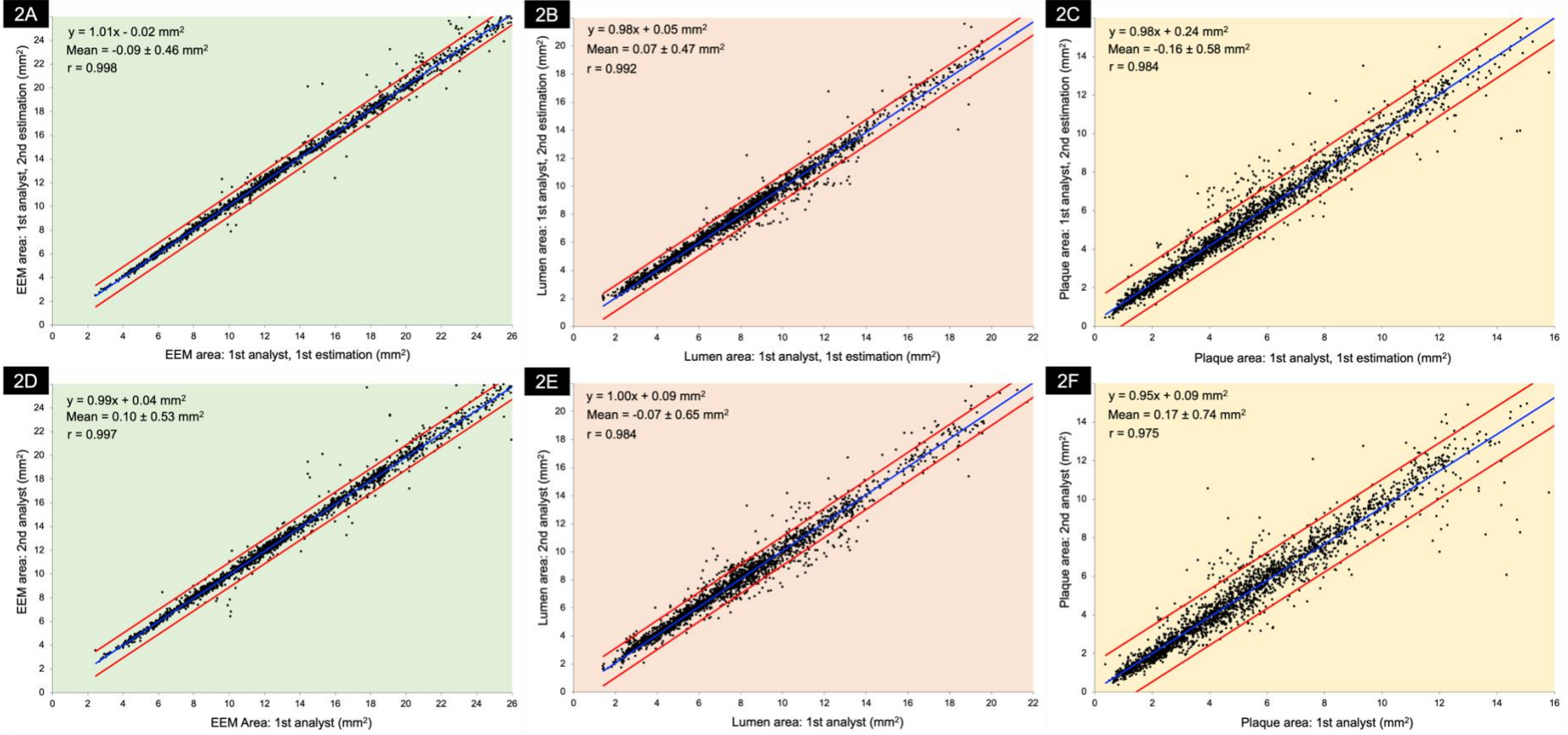
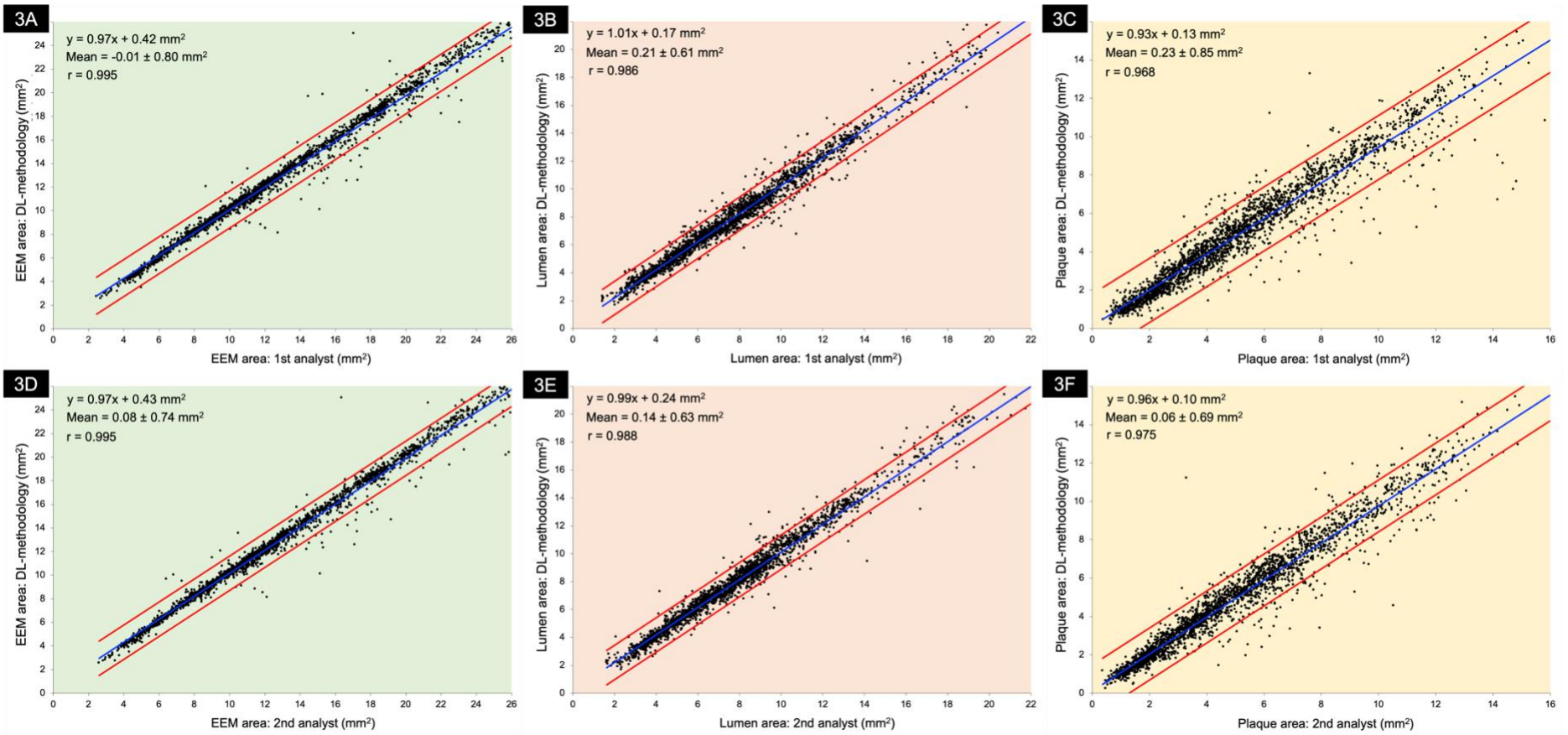


Figure 1.



**Figure 2.**



**Figure 3.**